



Kahramanmaraş Sutcu Imam University Journal of Engineering Sciences



Geliş Tarihi : 17.10.2025
Kabul Tarihi : 01.12.2025

Received Date : 17.10.2025
Accepted Date : 01.12.2025

INVESTIGATION OF WELDING CURRENT ON MECHANICAL AND CORROSION PROPERTIES OF TITANIUM-HYDROXYAPATITE TIG COATINGS ON Ti-6Al-4V BIOMEDICAL ALLOY

Tİ-6AL-4V BİYOMEDİKAL ALAŞIMI ÜZERİNE TİTANYUM-HİDROKSİAPATİT TIG KAPLAMALARIN MEKANİK VE KOROZYON ÖZELLİKLERİ ÜZERİNE KAYNAK AKIMININ ARAŞTIRILMASI

Muhammet Guman ÖZBEY¹ (ORCID: 0009-0004-5575-0252)
Mehmet TOPUZ^{2*} (ORCID: 0000-0003-3692-796X)

^{1,2} Van Yuzuncu Yil University, Department of Mechanical Engineering, Van, Türkiye

*Sorumlu Yazar / Corresponding Author: Mehmet TOPUZ, mehmettopuz@yyu.edu.tr

ABSTRACT

In this study, 5% hydroxyapatite (HA)-95% titanium (Ti) composite coatings were fabricated on Ti-6Al-4V (Ti64) substrates using the Tungsten Inert Gas (TIG) welding method at welding currents of 90A, 100A, and 110A. The effects of welding current on the microstructural, mechanical, electrochemical, and biological properties were systematically investigated. According to ASTM E190 bending tests, interfacial adhesion strength increased with increasing welding current. Electrochemical in vitro corrosion tests showed limited dependence on current, though the 100A coating exhibited the lowest corrosion current density ($6.93 \times 10^{-2} \mu\text{A} \cdot \text{cm}^{-2}$) and highest polarization resistance (12800 Ω), indicating the most passive surface behavior. In vitro simulated body fluid (SBF) tests demonstrated that the 90A coating promoted optimal apatite-like layer formation. Overall, the welding current strongly affected the coatings' microstructure, chemical stability, mechanical strength, corrosion resistance, and bioactivity. Among all, 90A was optimal for structural stability, 100A for electrochemical performance, and 110A for mechanical adhesion. Thus, the TIG welding process is a promising approach for producing biofunctional coatings on metallic substrates.

Keywords: Welding current, TIG coating, Ti-6Al-4V, adhesion, corrosion.

ÖZET

Bu çalışmada, %5 hidroksiapatit (HA)-%95 titanyum (Ti) kompozit kaplamalar, Tungsten İner Gaz (TIG) kaynak yöntemi kullanılarak 90A, 100A ve 110A kaynak akımlarında Ti-6Al-4V (Ti64) altlıklar üzerine üretilmiştir. Kaynak akımının mikroyapısal, mekanik, elektrokimyasal ve biyolojik özellikler üzerindeki etkileri sistematik olarak incelenmiştir. ASTM E190 eğme testlerine göre, arayüz yapışma mukavemeti artan kaynak akımıyla artmıştır. Elektrokimyasal in vitro korozyon testleri akıma sınırlı bağımlılık gösterdi, ancak 100 A kaplama en düşük korozyon akımı yoğunluğunu ($6.93 \times 10^{-2} \mu\text{A} \cdot \text{cm}^{-2}$) ve en yüksek polarizasyon direncini (12800 Ω) sergiledi ve en pasif yüzey davranışını gösterdi. İn vitro simüle edilmiş vücut sıvısı (SBF) testleri, 90A kaplamanın optimum apatit benzeri tabaka oluşumunu desteklediğini gösterdi. Genel olarak, kaynak akımı kaplamaların mikro yapısını, kimyasal kararlılığını, mekanik dayanımını, korozyon direncini ve biyoaktivitesini güçlü bir şekilde etkiledi. Hepsi arasında, 90A yapısal kararlılık için, 100A elektrokimyasal performans için ve 110A mekanik yapışma için optimumdur. Bu nedenle, TIG kaynak işlemi metalik yüzeylerde biyofonksiyonel kaplamalar üretmek için umut verici bir yaklaşımdır.

Anahtar Kelimeler: Kaynak akımı, TIG kaplama, Ti-6Al-4V, adhezyon, korozyon.

INTRODUCTION

Titanium (Ti) and its alloys are widely used in orthopedic implants due to their superior biocompatibility, high strength-to-weight ratios, and corrosion resistance. With these properties, it is an indispensable part of long-lasting and reliable orthopedic solutions. It is especially preferred in hip and knee prostheses, plates, screws, and dental implants (Niinomi, 2002). When Ti is exposed to body fluids, a nanometer-thick titanium dioxide (TiO₂) passivation layer spontaneously forms on its surface, minimizing ion release and ensuring long-term implant stability (Hodgson et al., 2002). Grade 4 pure titanium and Ti-6Al-4V (Ti64) alloy are specifically defined for implant production according to ASTM standards, characterized by alloy formulations containing 99% pure Ti and 6% aluminum (Al) - 4% vanadium (V), respectively. Especially the Ti64 ELI (Extra Low Interstitial) version is preferred in critical applications, such as spinal fusion implants, due to its increased fracture toughness, achieved by keeping impurities like oxygen and iron at controlled levels (Niinomi and Nakai, 2011). On the other hand, despite its advantageous properties, the presence of aluminum (Al) and vanadium (V) elements in its elemental composition poses a disadvantage for in-body use. The presence of the Al element within the body has been indicated to be associated with Alzheimer's disease in patients who have undergone implantation, according to clinical studies (Perl, 1985). The vanadium additive, frequently used as a beta (β) stabilizer element in Ti, enhances the mechanical properties of Ti, but its contribution to high osseointegration (body tissue integrity) in the biomaterial-tissue interaction is limited (Ji et al., 2020). For these reasons, current studies are being conducted on compositions and surface modifications that will enhance the tissue interaction between the biomaterial and the body (Benea et al., 2014; Mohseni et al., 2014).

At the forefront of these are Hydroxyapatite (HA) coatings due to their elemental and structural similarity to bone tissue. One of the most important components of biomaterial research, HA is a calcium phosphate compound that constitutes the inorganic phase of natural bone tissue (Topuz et al., 2024a). This ceramic material, which shows extraordinary compatibility with biological systems, exhibits biocompatibility, osteoconductivity, and osteointegration properties due to its chemical structure similar to that of bone tissue (Breding et al., 2014). Especially in orthopedic and dental implant applications, the high bioactivity of hydroxyapatite improves biomechanical stability by enhancing the integration at the implant-soft tissue interface. With these properties, HA is widely used in critical applications such as bone graft alternatives, dental implant coatings, and tissue engineering scaffolds (Topuz et al., 2024b; Topuz et al., 2021b). However, the disadvantage is the presence of cases where HA's mechanical rigidity alone is insufficient (Topuz et al., 2023; Topuz et al., 2021a). This disadvantage is due to the weak chemical interaction between HA's ceramic (bioceramic) structure and the metallic biomaterials used as the base material. As a result of the weak chemical interaction, there is insufficient coating adhesion between the metallic and ceramic coatings. Therefore, researchers continued to produce composite coatings with different metallic material reinforcements to enhance the weak interfacial strength of HA in coatings (Topuz et al., 2025). Composite biomaterials continue to revolutionize the fields of engineering and medicine. Deepening research in this field contributes to the development of safer and more effective biomaterials (Geetha et al., 2009). The clinical applications of composite biomaterials span a wide range. In orthopedic surgery, calcium phosphate ceramics and polymer composites are used to repair bone-based defects. Composites containing hydroxyapatite provide structures that can integrate with natural bone by promoting the proliferation of bone cells (Eriksson et al., 2006).

For the reasons mentioned, scientists have applied Ti-HA coatings to the surface of Ti64 using different coating methods (Mohseni et al., 2015). One of the main issues in biomedical coatings, which have different advantages and disadvantages, can be said to be the insufficient adhesion strength between the coating and the substrate material. To prevent this issue, commercial methods such as plasma spray are currently used; however, these methods are costly due to their high initial investment costs and complex operating conditions (Dikici et al., 2016). For these reasons, next-generation laser cladding applications have been developed, but different searches continue to be pursued considering the cost-benefit balance (Hu et al., 2021; Weng et al., 2014). The coating structures obtained through the Tungsten Inert Gas (TIG or GTAW: Gas Tungsten Arc Welding) method promise an alternative as a result of these explorations. TIG welding is a high-precision welding method widely used in industries that require superior weld quality, such as aerospace, nuclear engineering, automotive manufacturing, and medical device production. Unlike other arc welding methods, TIG welding uses and/or does not use a non-consumable tungsten electrode, and the molten weld pool is protected by an inert shielding gas to prevent atmospheric contamination. This process is known for its ability to produce clean, spatter-free welds and provide excellent mechanical properties along with an aesthetically pleasing appearance (Lucas, 1990). Considering its role in critical applications, understanding fundamental parameters such as current settings, shielding gas selection, electrode types, and advanced techniques is of great importance for optimizing welding performance (Biswas and Sahoo, 2023).

Many studies have been conducted on Ti64 surfaces for various purposes using the TIG welding method. For example, Tijo and Masanta (Tijo and Masanta, 2019), in their research, stated that the XRD spectra of the coating samples prepared at lower currents (50A and 70A) were almost the same when using a powder mixture of titanium (Ti) and boron carbide (B_4C) with different weight ratios pre-placed on a Ti64 substrate for TIG coating. An et al. (An et al., 2017) similarly produced TIG coatings of pre-sintered 11.8% $TiB_2/Ti64$ composites on Ti64. With the increase in heat input (i.e., welding current), the TiB content decreased, and the coating's microstructures became more homogeneous, while the hardness values decreased. Waghmare et al. (2018, on the other hand, have applied Ni_xTi_y ($NiTi$ and $NiTi_2$) coatings on Ti64 surfaces using the TIG coating method. They stated that the TIG process current has a significant impact on the morphology and mechanical properties of the coating layer and that with a low current input (40A and 50A), the hardness value increases while the wear value decreases. In most of the conducted studies, the aim was to obtain hard surfaces, and in this direction, hardness and wear values were systematically examined (Bansal et al., 2020; Saroj et al., 2017). However, no study has been found that aims to improve the biological surface properties of Ti64 (potential biomaterial use) using the TIG cladding method.

The novelty of this study lies in the systematic investigation of how welding current affects the mechanical integrity and in vitro corrosion behavior of Ti-HA composite coatings fabricated on Ti-6Al-4V substrates via the TIG cladding method. Unlike previous TIG-based studies focused mainly on hardness or wear resistance, this study targets biomedical functionality by enhancing bioactivity and corrosion resistance. The study also establishes a clear relationship between welding current, coating microstructure, and electrochemical performance, offering a cost-effective and scalable alternative to conventional coating techniques. The morphological and structural characterizations of the produced composite surface coatings were revealed using various techniques. The adhesion strength between the coating and the substrate material was determined through bending tests (ASTM E190). Moreover, the electrochemical in vitro corrosion responses of the surface coatings were revealed in detail by using the three-electrode technique.

MATERIALS AND METHODS

Ti and HA powders were weighed on a precision scale (Shimadzu, TX423L). HA (approximate particle size $\sim 25-50 \mu m$) and Ti-based (approximate particle size $\sim 45 \mu m$) composites were mixed for about 30 min to obtain a slurry mixture with a 5% by vol. HA fraction. The HA content was fixed at 5% for two critical reasons. Firstly, higher HA concentrations can introduce thermal barrier effects during TIG welding, which may hinder metallurgical bonding and promote porosity formation within the coating. Secondly, excessive HA fractions are prone to thermal decomposition under elevated welding currents, compromising the phase stability and integrity of the composite layer. Therefore, to ensure optimal adhesion, structural uniformity, and compositional stability, the HA content was maintained at a constant level of 5%. To ensure a homogeneous mixture of the slurry, ethyl alcohol was used. The obtained slurry was first dried in an atmospheric environment and then in an oven (at $120^\circ C$ for 45 min). As a result of the process, the moisture and alcohol content within the slurry have been evaporated. The dried Ti-HA composite powder mixture was pressed to ensure that the homogeneity of its surface distribution was not affected by the welding atmosphere gas. The pellets were produced using a stainless-steel cylindrical mold ($\varnothing 10$ mm) under a pressure of 250 MPa for 45 s using a uniaxial hydraulic press (Carver, Model 4555).

TIG Coating Procedure

The Ti64 alloy plate, sized $50 \times 150 \times 4$ mm, was cut into 20 pieces using a hydraulic press and subjected to a cleaning process with ethyl alcohol, acetone, and distilled water for 5 min each before the TIG welding process. The Ti-HA composite pellets were coated onto the Ti64 alloy under an argon (Ar) protective atmosphere. The TIG coating process was carried out using a tungsten electrode with a diameter of 2.4 mm, optimum protection was provided with an Ar gas flow of 18 L/min, and the risk of oxidation was minimized. As welding parameters, current intensities of 90A, 100A, and 110A were used. A controlled welding process with low heat input was applied to create a homogeneous melting zone at the pellet-alloy interface. The composite-coated Ti64 was then allowed to cool in an atmospheric environment. With the TIG coating method, the Ti-HA composite pellets were coated onto the substrate with high adhesion and homogeneity.

After the TIG coating process was completed, grinding and polishing operations were carried out to remove the welding spatter in the joint area and reduce surface roughness. In the first stage, coarse grinding was performed using the coarse grinding machine (KLPRO, KLTM175), and the prominent protrusions around the weld seam were removed. Subsequently, a series of sandpapers was applied in succession with grids of 240, 400, 600, and 800 to enhance the surface quality. In the final stage, a polishing process using a diamond suspension (with 6, 3, and 1 μ

cloth) was applied to achieve a mirror-like appearance on the coating-substrate zone. During all processes, low rotational speeds were used to prevent overheating and microstructural changes in the sample, and periodic cooling with water was provided. As a result of these surface preparations, a surface quality suitable for microscopic examinations was achieved, and the samples met the standard requirements before mechanical testing.

Characterization

An optical microscope (OM) was used to observe the microstructure formed after the coating process, and especially the thermal effects. To examine the surface morphology in more detail, a field-emission scanning electron microscope (FE-SEM, Zeiss, Sigma 300) was preferred. Elemental analyses of the samples coated with energy-dispersive X-ray spectroscopy (EDX, Ametek, EDAX) integrated into the SEM device were conducted. X-ray diffraction (XRD) analyses were performed employing Cu-K α radiation ($\lambda = 1.5406 \text{ \AA}$) over a 2θ range of 10° – 90° , with a step size of 0.2° to determine the phase structures occurring in the composite coatings. Within the scope of these analyses, it was investigated whether the thermodynamic interactions occurring between Ti64-Ti, Ti64-HA, and Ti-HA, particularly as a result of HA reinforcement, lead to the formation of new phases. Additionally, the wettability properties of the surfaces were evaluated by measuring the contact angles (Attension, Theta Flex) between the surfaces coated with simulated body fluid (SBF). As a result of these measurements, the surface properties that Ti64 surfaces coated with different ratios of Ti-HA can exhibit in potential in-body applications, particularly their wettability degrees, have been revealed.

Bending Tests for Adhesion Evaluation

Longitudinal face bend tests were conducted following ASTM E190 standards to determine the adhesion strengths between the composite coatings and Ti64. In this way, it has been determined at what load and deformation the coatings will detach from the surfaces. The samples with a cross-section dimension of $30 \times 4 \text{ mm}$ were used in longitudinal face bend tests for the evaluation of adhesion at the coating interface. The tests were carried out from the back of coatings at a speed of $0.2 \text{ mm} \cdot \text{min}^{-1}$. The deformation mechanisms that may occur have been examined and interpreted with the help of macro images from the cross-section of fractured surfaces.

Electrochemical In Vitro Corrosion Tests

Electrochemical in vitro corrosion tests were conducted to determine the corrosion resistance of the produced Ti-HA composite coatings, using a computer-controlled potentiostat-galvanostat (Palmsens, Emstat 4R). In all electrochemical in vitro corrosion tests, a three-electrode technique was used. Here, a saturated silver/silver chloride electrode (Ag/AgCl) was used as the reference electrode (RE), a platinum wire (Pt) as the counter electrode (CE), and Ti-HA composite coatings were used as the working electrode (WE) for the test. Within the scope of the study, various electrochemical in vitro tests were conducted to fully determine the in vitro corrosion behavior of Ti-HA composite coatings. These are open circuit potential (OCP) changes, potentiodynamic polarization (PDP) tests, and electrochemical impedance spectroscopy (EIS) tests. During the OCP conducted here, the aim was for the composite coatings to become stationary within the SBF, while the corrosion current densities (I_{corr}), an important parameter, were obtained through the PDP tests. Additionally, the surface layer behavior of the coatings about the SBF was revealed through EIS tests. The tests were repeated under in vitro conditions (in SBF electrolyte at body temperature, $\sim 37^\circ\text{C}$), and the passivation tendencies of the coatings were revealed. During the electrochemical in vitro corrosion tests, 1 cm^2 of each coating was exposed to SBF with cold mounting to prepare the WE. Initially, OCP measurements were conducted for 2400 s to ensure a steady-state potential for the SBF electrolyte. Subsequently, PDP tests were carried out, commencing from a cathodic overpotential of -2.0 V relative to OCP potential and scanned anodically at a potential sweep rate of $1 \text{ mV} \cdot \text{s}^{-1}$ until reaching $+3.0 \text{ V}$. Finally, EIS analyses were conducted to comprehensively elucidate the electrochemical behavior of the coatings in the SBF. The EIS measurements were performed using a sinusoidal AC perturbation of 10 mV amplitude over a frequency spectrum ranging from 100 kHz to 0.01 Hz .

In Vitro Bioactivity Tests

SBF immersion tests were conducted to measure the ability of the produced composite coatings to form apatite (apatite: bone-like tissue) on their surfaces, namely bioactivity tests. After the SBF immersion process, the samples were dried in a desiccator without any heat source. The formation of apatite on the surface of the composite coatings was observed using SEM. In SEM surface examinations, a thin metal coating (Au-Pd) was applied to induce the electrical conductivity of the composite coatings. The SBF solution is an artificial body fluid prepared based on the ionic composition of human blood plasma, allowing for the imitation and observation of bone-like apatite formation on the biomaterial surface. Developed by Kokubo and Takadama (Kokubo and Takadama, 2006), this solution has become a widely used method for evaluating the biocompatibility and functionality performance of materials in an

in vitro environment. The SBF electrolyte consists of the chemicals NaCl, KCl, CaCl₂, MgSO₄·7H₂O, MgCl₂·6H₂O, Na₂HPO₄·2H₂O, 4KH₂PO₄, D-glucose (dextrose), and NaHCO₃. The required chemical amounts to prepare 1000 mL of SBF are 8 g, 400 mg, 140 mg, 100 mg, 100 mg, 60 mg, 60 mg, 1 g, and 350 mg.

RESULTS AND DISCUSSIONS

Macro cross-sectional images of composite surface coatings performed on the Ti64 alloy using the TIG welding method are given in Figure 1. In all coatings, a distinct transition zone between the weld zone and the Ti64 base metal has been observed. This transition zone exhibits melting and recrystallization behavior resulting from the effect of heat input. In Figure 1a, with a 90A welding current, the weld zone is narrower and more distinct, and it has been determined that it merges under a limited heat effect with the base metal. This situation suggests that it may have occurred with a relatively low welding current or a short duration of heat input (Buytoz et al., 2005). Although coating continuity has been achieved, the boundaries of the weld zone are clear and symmetrical. In Figure 1b, in the coatings performed with a 100A welding current, the weld zone has expanded, and a more homogeneous melting and fusion behavior has been observed both horizontally and vertically. This situation indicates a structure obtained with an optimal level of welding parameters. At the same time, no delamination or void formation has been observed at the coating-substrate interface. These characteristics indicate that the coating has a high adhesion strength as a biomaterial. The coating produced with an 110A welding current, as shown in Figure 1c, has a welding area that is much larger, and under significant heat input, melting and mixing are observed in both the base metal and the coating area. This situation may have occurred due to a high welding current or prolonged heat input (Kumar and Masanta, 2023). However, in this example, irregular phase distribution impressions can be observed. In all sections, the characteristic structure of the Ti64 substrate metal is preserved; however, the shape and width of the weld zone vary significantly depending on the applied welding parameters. Especially in the 100A sample, the homogeneous weld zone observed represents the most successful result in terms of biomaterial performance.

The surface properties of composite coatings were given in terms of OM images, as shown in Figure 1. It was observed that ceramic particles were distributed on the surface at a microscopic scale with the 90A welding current. In this sample, the coating integrity has generally been preserved, and a balanced transition between the ceramic and metal matrix has been achieved. In the 100A sample, it was observed that the optical images had the most homogeneous distribution. Ceramic particles were evenly distributed on the surface and formed a good bond with the metallic structure. A controlled HA distribution may be achieved. In the case of sample 110A, the integration of HA ceramics to the surface may result in local failures that may be observed, which can reduce the biological functionality of the surface. As a result of OM analyses, the coating obtained under 100A current has provided the most balanced and successful outcome in terms of surface homogeneity, phase transitions, and overall integrity. This demonstrates suitability, particularly in terms of the balanced HAZ region (Aslam et al., 2023), for biomaterial applications.

In Figure 2, the surface morphologies of the composite coatings were examined using SEM. As seen in Figure 2a, ceramic HA particles with a dispersed structure were observed on the surface with 90A (the dark areas in the coating regions). These particles are irregularly but dispersedly located on the Ti matrix, indicating that HA is retained on the surface with its non-melting structure during the welding process. Some micropores and partial bonding regions have been detected at the edges of the particles. On the other hand, in Figure 2b, it was observed that the ceramic phases were more homogeneously distributed within the Ti matrix, the particle sizes were more stable, and the integration with the surface was successful. The welding parameters successfully integrated the HA structure onto the surface without causing any damage. At the same time, fewer cracks and lower porosity were observed on the surface. With the 110A welding current, it was observed that in some areas, ceramic particles melted or fragmented due to the high current (Shbeh et al., 2019). These findings indicate that high heat input can disrupt the HA structure, negatively affecting its biological performance (Figure 2c). Overall, the 110A welding current presented the most successful and homogeneous structure in terms of surface morphology, which positively affected the functional performance of the coating as a biomaterial.

The elemental compositions of the obtained coatings were given with EDX analyses in Figure 2-EDXs. In the 90A sample, Ca and P elements were revealed with EDX analyses. This situation indicates that the low welding heat input partially succeeded in integrating ceramic particles onto the surface, but the ceramic phases could not remain fully stable on the surface (Figure 2EDXa-b). In the 100A sample, it was observed that the Ca and P elements were densely present on the surface, indicating that the ceramic maintained its biologically active structure and bonded compatibly with the Ti matrix (Figure 2EDXc-d). It was determined that some HA phases dissociated due to the high-temperature

effect in Ca and P concentrations observed with the 110A welding current (Nath et al., 2009). Chemical stability can be adversely affected by high energy input (Figure 2EDXe-f). In conclusion, EDX analyses have shown that the 90A welding current parameter provides the most suitable conditions for the chemical stability of HA phases and their integral surface integration.

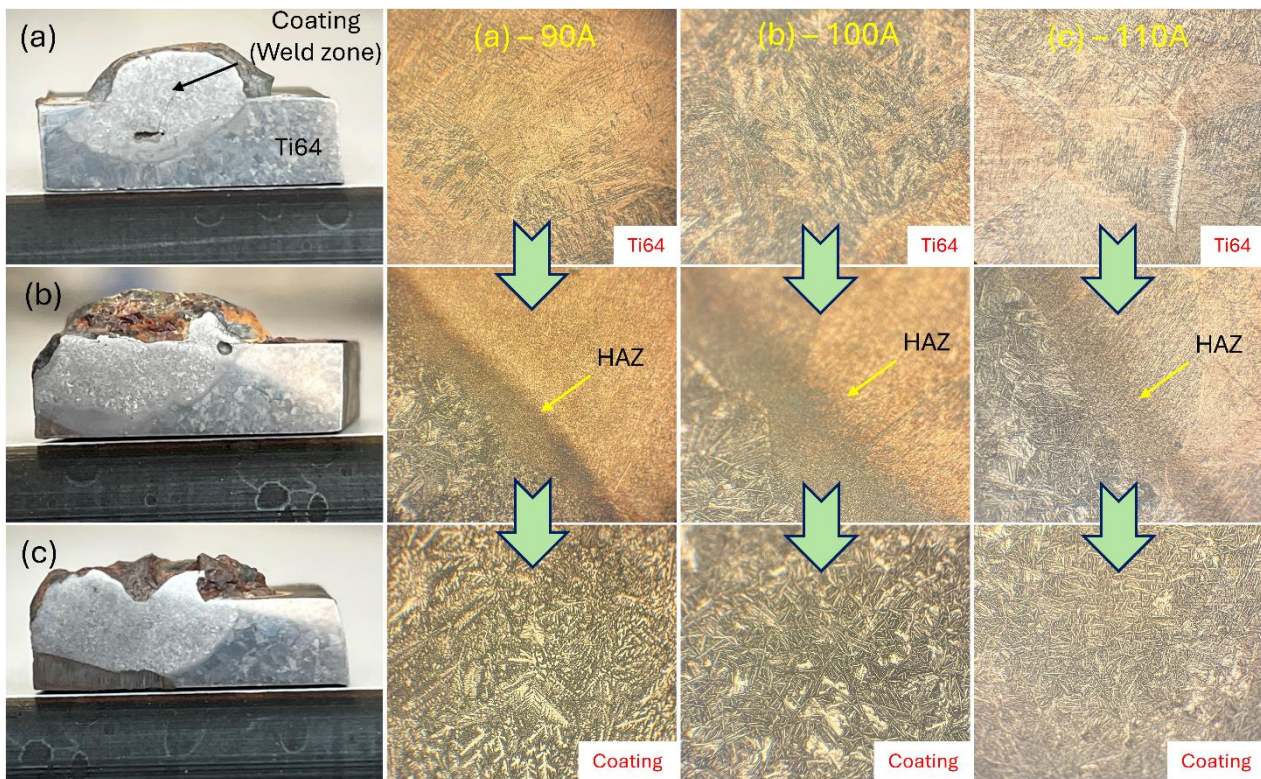


Figure 1. Cross-Sectional Macro Images and Detailed OM of TIG-Coated Ti64 Surfaces: (a) 90A, (b) 100A, and (c) 110A.

The analysis of the XRD under different welding currents is given in Figure 3. At a current of 90A, characteristic peaks of Ti (β -Ti at around 35° , 38° , 40° , etc. 2θ) were observed alongside intense peaks of HA phases (characteristic peaks at 35° , 38° , 40° , 53° , 63° , 70° , 76° , and 82° 2θ) (Ebrahimi et al., 2018; Qiu et al., 2011). This situation indicates that the low heat input partially preserves the crystal structure of HA. It is observed that the characteristic peaks of HA gradually decrease, and Ti becomes dominant (100A sample). This indicates that the crystal structure of HA may relatively deteriorate and evolve into different components (CaTiO_3) with the increasing welding current. However, no clear signs of any phase transformation or secondary phase formation have been definitively observed. A decrease in the intensity of HA peaks and peak broadening in some regions has been observed within the 110A sample. This situation suggests that HA is partially degraded by the high-temperature effect, tending to form secondary phases such as amorphization or calcium titanate (CaTiO_3) (Nath et al., 2009). The 100A welding current has been evaluated as the most suitable parameter in terms of preserving the crystal structure of HA, phase stability, and compatibility with the Ti matrix. Because, although HA may undergo partial degradation with this welding current, it can exhibit improved mechanical properties compared to 90A (Figure 4). Generally speaking, it has been determined that this parameter (90A) provides the ideal crystal phase balance.

In Figure 4, the mechanical adhesion strengths of the composite surface coatings were evaluated using a three-point bending test (ASTM E190). The force-deformation curves of the reference Ti64 sample were comparatively analyzed with the samples obtained at different welding currents (90A, 100A, 110A). The Ti64 reference sample reached a maximum force value of approximately 2.42 kN and exhibited a high deformation capability with a ductile character. This situation reveals the natural strength characteristics of the alloy. The sample coated with 90A reached a maximum force value of approximately 1.43 kN and exhibited a more brittle behavior compared to the reference sample. On the other hand, due to the low energy input, the coating integrity remained limited, and the mechanical performance significantly decreased. The sample coated with 100A exhibited moderate bending strength at approximately 2.12 kN. This sample exhibited the most balanced mechanical behavior with both high load capacity and good deformation capability. The homogeneous distribution of HA within the Ti matrix and sufficient welding

energy have enhanced the coating integrity. The sample coated with 110A reached a maximum force level of 2.26 kN, increased its deformation capacity, and exhibited brittle fracture behavior. This situation is thought to be due to the high heat input providing a more homogeneous transition at the coating interface and causing phase separations, leading to the formation of stronger bonds between Ti and Ti64 (Mohseni et al., 2015). The coatings obtained with an 110A welding current offered the most suitable parameter combination in terms of mechanical strength and deformation capability.

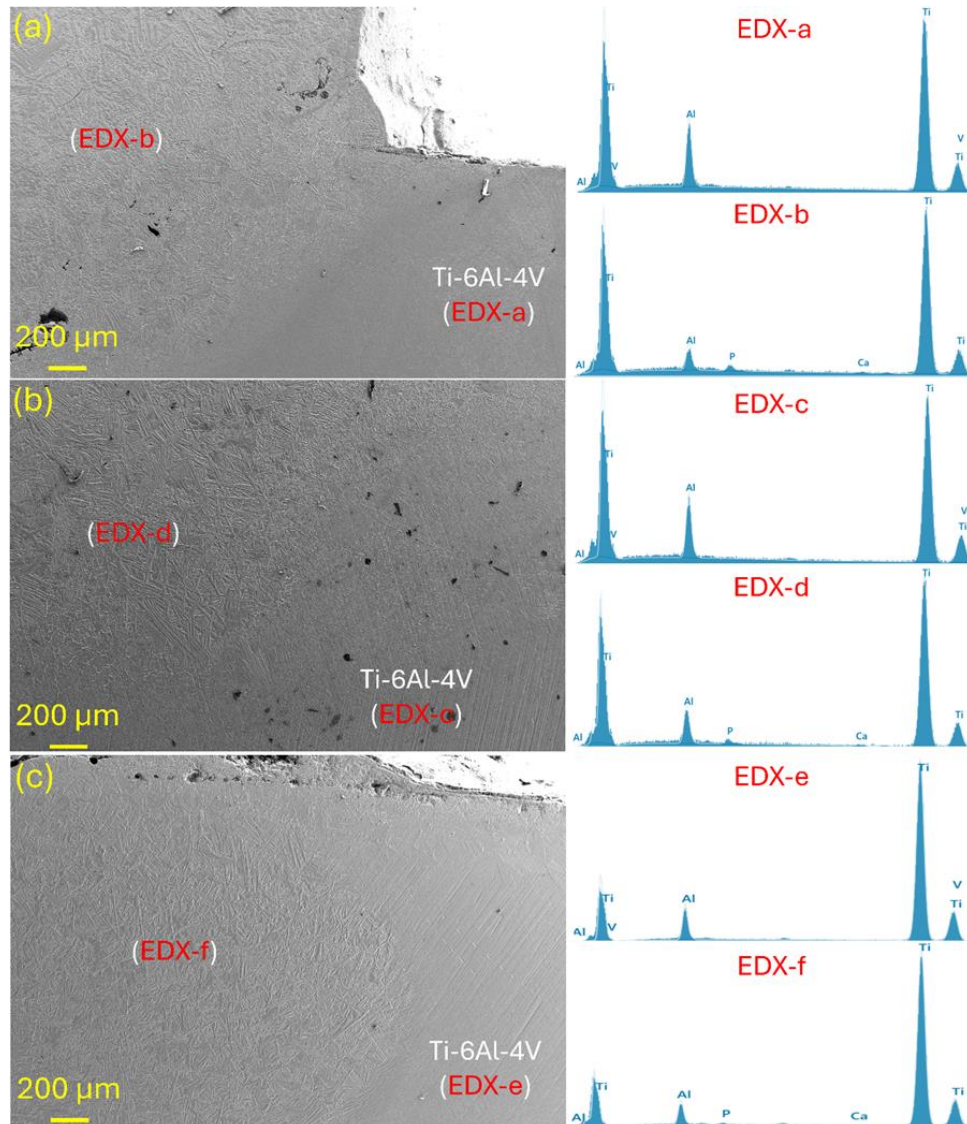


Figure 2. SEM Morphology Examinations Taken from the Interfacial Surfaces of the Coatings: (a) 90A, (b) 100A, and (c) 110A. The EDX Analysis Results Obtained from the Points Shown in the SEM Micrographs Represent (a,c,and e) Ti64 and (b,d,and f) Composite Coating Sections.

In Figure 4, the fracture surface morphologies after bending tests have also been evaluated. No particle separation traces were found on the fracture surface of uncoated Ti64. This confirms the homogeneity of the alloy and the absence of any additive material in its internal structure that would cause embrittlement. The fracture surface has a structure that is relatively smooth and contains a small number of fracture areas (90A sample). This can occur due to limited bonding quality, which occurs due to low source energy, and the delamination occurs at the coating-substrate interface. It has been observed that microstructural discontinuities are not widespread, but adhesion remains weak (Padhee et al., 2020). In the 100A sample, dense micro-cracks and irregular fiber-like structures were observed on the fracture surface. The high energy input has successfully integrated HA particles into the matrix, and the energy absorption under stress is higher compared to 90A. The fracture has a ductile-brittle mixed character, and the mechanical integrity of the coating is moderate. In the case of sample 110A, the fracture surface is brittle in nature; there are distinct crack lines and sharp fracture planes along the surface. Due to excessive energy input, internal stresses have formed in the coating structure, the HA phase has been partially decomposed, and the coating has higher

adhesion than other welding currents due to the more Ti-Ti64 bonding. It was determined that the 110A welding current parameter was the most effective in mechanically bonding HA to the matrix and exhibited ductile fracture behavior under deformation.

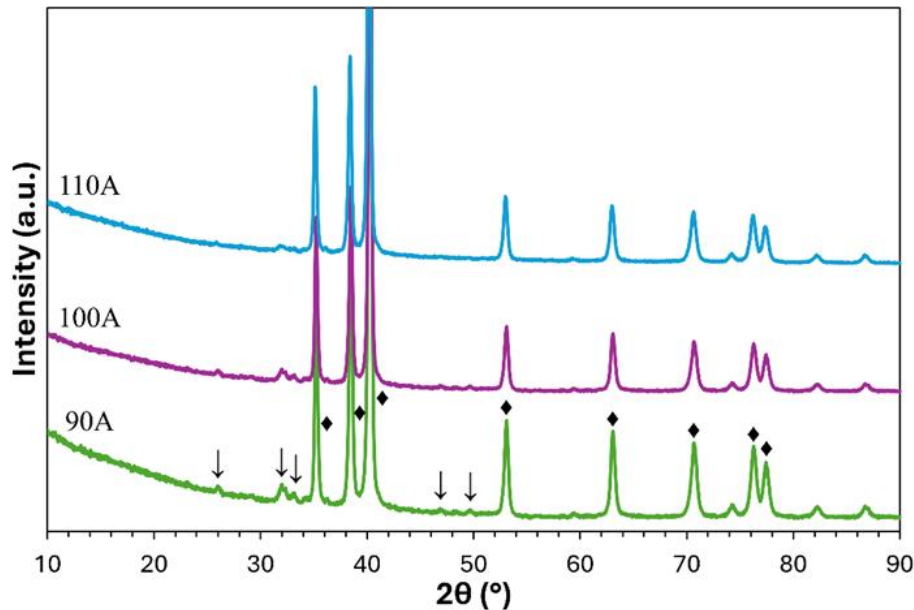


Figure 3. XRD Analysis Results of Samples, ↓: HA, and ♦: Ti.

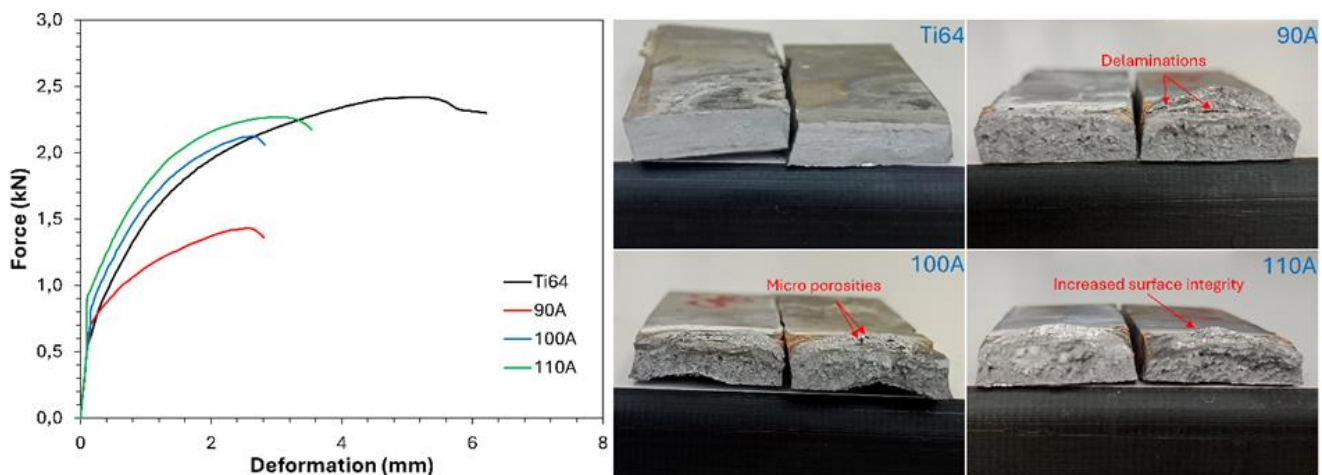


Figure 4. Bending Test Results of Uncoated Ti64 and Composite Coatings with Detailed Fractured Surfaces.

In Figure 5a, the steady state of the composite surface coatings in the immersed SBF electrolyte was evaluated using the OCP test. OCP curves provide important information about passive film formation and electrochemical stability. At a 90A welding current, the initial potential value, although at a level similar to 100A, has shown significant fluctuations over time. It is understood that the high energy input disrupts the structure of HA, weakening the integrity of the passive film, and this condition limits the corrosion resistance (Schultze and Lohrengel, 2000). At a 100A welding current, the OCP value was initially around -0.60 V and showed only a slight increase over time. This situation indicates that the formation of a passive film is limited and that the surface is not sufficiently resistant to corrosion. Low energy input was not sufficient for HA to form a stable structure on the surface. At an 110A welding current, the initial OCP value was more positive and showed a more stable trend over time. It has been evaluated that a stable passive film forms on the surface and that lower HA shows a higher protective effect in the electrochemical environment (Tozkoparan et al., 2020). Because HA ceramic particles behave as a corrosion path for low wettability between the Ti matrix, this parameter (110A) has provided the most balanced and successful result in terms of the coating's corrosion resistance at steady states.

The polarization scans of samples obtained at different welding currents (90A, 100A, 110A) were evaluated, and their corrosion current densities (I_{corr}) and corrosion potentials (E_{corr}) were given in Figure 5b. The important electrochemical corrosion parameters obtained from Tafel extrapolation in PDP curves are given in Table 1. At a welding current of 90A, the I_{corr} value was measured at the highest level ($2.32 \times 10^{-2} \mu\text{A} \cdot \text{cm}^{-2}$), indicating insufficient passive layer formation on the surface and a high tendency for corrosion. The polarization curve has fluctuated at negative potential values, indicating low corrosion resistance. At a 100A welding current, the I_{corr} value reached a relatively low level ($6.93 \times 10^{-2} \mu\text{A} \cdot \text{cm}^{-2}$) and the potential value showed a more negative trend. This result may indicate that the welding parameters ensure the balanced integration of HA onto the surface, meaning that the balance of a stable and protective passive film in the coating has been deformed with increased potential scanning. At an 110A welding current, the I_{corr} value decreased even further compared to 100A ($8.74 \times 10^{-2} \mu\text{A} \cdot \text{cm}^{-2}$), and the curve exhibited a more unstable (anodic region) behavior. Structural damage caused by high-energy input has weakened the coating integrity and negatively affected corrosion resistance. PDP curve data has shown that the 100A welding current combination offers the lowest I_{corr} and the highest electrochemical resistance (Tozkoparan et al., 2020). This situation offers a long-lasting and safe protective surface in terms of biomaterial applications.

The electrochemical corrosion resistance of the composite coatings was evaluated using the EIS-Nyquist method and is given in Figure 5c. The obtained Nyquist curves (Z' vs $-Z''$) were comparatively analyzed through samples prepared with different welding currents (90A, 100A, 110A). The Nyquist plot is in the form of a semicircle with a small radius, indicating low charge transfer resistance (90A sample). This situation indicates that the low energy input is insufficient to ensure coating integrity and that passive film formation is weak. At a 100A welding current, the curve radius is larger than at 90A, increasing electrochemical resistance. The high current reduces irregularities in the coating structure and positively affects the formation and continuity of the passive layer. 110A welding current, the Nyquist curve with the largest semicircle was obtained. In this sample, the charge transfer resistance occurred at the highest level, and it was determined that the coating offered maximum resistance to corrosion (Topuz and Teter, 2025). The stable passive film formed on the surface has exhibited a highly resilient structure in the electrochemical environment. Nyquist plots have shown that the combination of 110A welding current provides the highest charge transfer resistance with the widest impedance curve radius, thereby demonstrating the strongest corrosion resistance (Topuz, 2023b). This has been identified as the most suitable parameter for long-term electrochemical stability in biomaterial applications.

The surface hydrophilicity of uncoated Ti64 and composite-coated surfaces was given in Figure 6 in terms of contact angle measurements. On the Ti64 reference surface, the contact angle was determined to be one of the highest values (mean $\sim 91.60^\circ$), and it was observed that the surface had a more hydrophobic character. This situation indicates that the metallic surface has low surface energy and limited cell adhesion potential (Menzies and Jones, 2010). In the case of sample 90A, the contact angle remained relatively high (mean $\sim 80.08^\circ$), indicating that the surface is only mildly hydrophilic. Due to the low welding current, the HA did not distribute homogeneously on the surface, causing irregular roughness and lower wettability. In the 100A sample, the contact angle reached its lowest level (mean $\sim 56.87^\circ$), and the hydrophilic character of the surface became more pronounced. This situation indicates that the surface energy has increased due to the smooth integration of HA onto the surface, resulting in a more biologically active structure. This state of the surface provides ideal conditions for osteoblast cell adhesion and proliferation (Topuz and Topuz, 2025; Mehl et al., 2016). In the 110A sample, the contact angle was higher (mean $\sim 59.72^\circ$) compared to the 100A sample. This increase can be attributed to the high welding energy disrupting the microstructural integrity of HA and reducing surface continuity. The microscopic cracks and pores formed on the surface may have caused an increase in the contact angle. Overall, contact angle measurements have shown that the 100A welding current parameters increase the surface's hydrophilic character the most, thereby enhancing its potential for biological activity.

In Figure 7, the biological activity potential of the composite surface coatings was evaluated through immersion tests conducted in simulated body fluid (SBF). In the 90A sample, irregular and localized calcium phosphate (Ca-P) deposits were observed on the surface. Due to the low source current, an adequate amount of HA active region formed on the surface, which is required for better osseointegration capacity (Topuz, 2023a). Extensive areas of the surface were found to be covered with dense and homogeneous morphologically apatite deposits (100A). HA is effectively integrated onto the surface and exhibits osteoinductive characteristics in the SBF environment. The smooth apatite crystals on the surface demonstrate that they provide a highly favorable environment for bone cell adhesion and the formation of bone-like structures. In the 110A sample, the Ca-P formations on the surface remained sparser and more fragmented. It has been evaluated that the high source current may decompose the HA crystal structure, reduce

nucleation sites, and limit the capacity for apatite formation. The 90A welding current has been shown to promote the formation of bone-like apatite in a biological environment most intensely and regularly. This situation can additionally be explained by the partial degradation of HA in the EDX analyses (Figure 2). Indeed, it is thought that the Ca-P formations on the surface may have formed irregularly as a result of the degradation of HA with the increased current flow (110A>100A). Coatings performed with 90A stand out as the most suitable combination for supporting bioactivity on implant surfaces as a biomaterial.

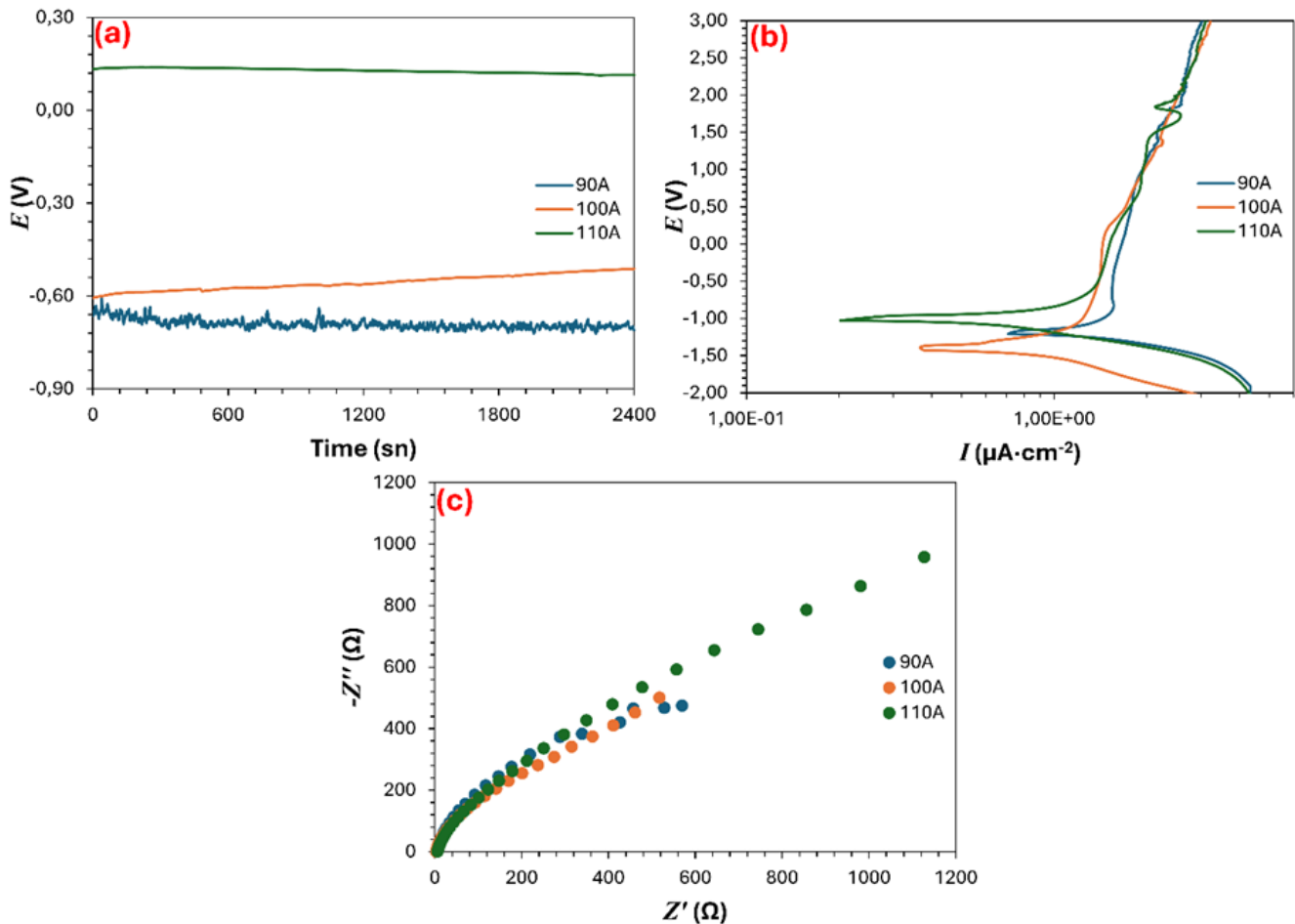


Figure 5. Electrochemical In Vitro Corrosion Results of Coatings, (a) OCP Immersion, (b) PDP Curves, and (c) EIS-Nyquist Curves.

Table 1. Some Important Corrosion Parameters from PDP Curves

Coating	E_{corr} (V vs, Ag-AgCl)	I_{corr} ($\mu A \cdot cm^{-2}$)	R_p (Ω)	β_a ($V \cdot dec^{-1}$)	β_c ($V \cdot dec^{-1}$)	Corr. rate ($mm \cdot year^{-1}$)
90A	-1.173	2.32×10^{-2}	2943	3.763	0.234	0.203
100A	-1.431	6.93×10^{-2}	12800	2.007	0.335	0.061
110A	-1.160	8.74×10^{-2}	6789	1.989	0.212	0.077

CONCLUSION

This study comprehensively examined the properties of composite surface coatings applied to the Ti64 alloy using the TIG welding method under different welding currents of 90A, 100A, and 110A. As a result of the analyses conducted, it was determined that the 100A welding current provided the most homogeneous welding region and ceramic particle distribution in the coatings, preserved the biologically active structure of HA, and exhibited the most balanced mechanical performance. Additionally, the surfaces coated with 100A exhibited the most hydrophilic character, showing high bioactivity potential with dense, homogeneous apatite accumulation, as well as enhanced corrosion resistance. On the other hand, the 90A welding current was found to be suitable in terms of the chemical

stability and surface integration of HA and supported the formation of bone-like apatite; however, its mechanical properties remained limited. The 110A welding current, although exhibiting the highest adhesion strength, negatively affected the biological functionality due to the high heat input, causing disruptions in the HA structure. In conclusion, it has been revealed that different welding currents possess different properties and that by using specific welding currents according to needs, various advanced properties, such as mechanical and corrosion-resistant, can be imparted.

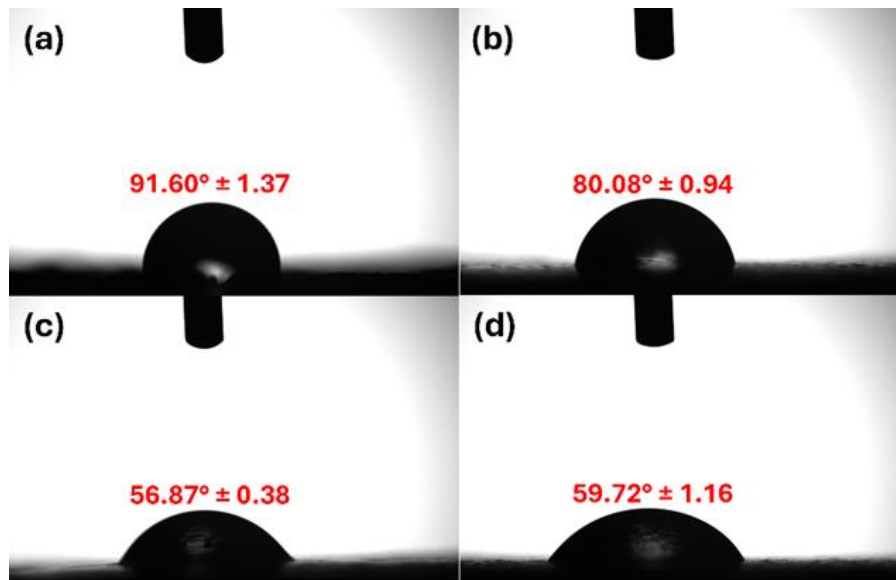


Figure 6. Contact Angle Measurement Results of the Sample: (a) Ti64, (b) 90A, (c) 100A, and (d) 110A.

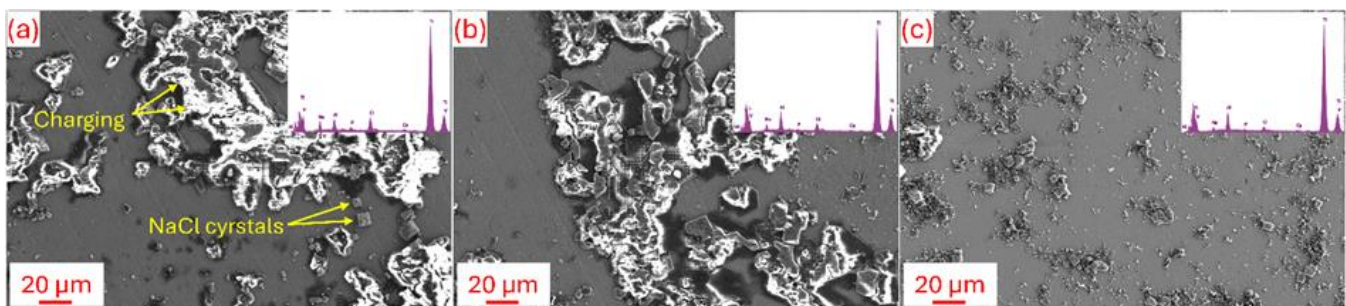


Figure 7. SBF Bioactivity Results of Samples (a) 90A, (b) 100A, and (c) 110A.

Acknowledgement

The authors would like to thank Van Yuzuncu Yil University, Scientific Research Projects Coordination Unit (Project no: FYL-2024-11226) for the financial support of this study.

Artificial Intelligence Contribution Statement

This manuscript was entirely written, edited, analyzed, and prepared without the assistance of any artificial intelligence tools. All content, including text, data analysis, and figures, was solely generated by the authors.

REFERENCES

- An, Q., Huang, L., Jiang, S., Li, X., Gao, Y., Liu, Y., & Geng, L. (2017). Microstructure evolution and mechanical properties of TIG cladded TiB reinforced composite coating on Ti-6Al-4V alloy. *Vacuum*, *145*, 312–319. <https://doi.org/10.1016/j.vacuum.2017.09.019>.
- Aslam, M., Chandan, G. K., & Kanchan, B. K. (2023). Development of SiC Ceramic Reinforced Composite Interlayer Cladding with AISI304 Stainless Steel Wire on Low Carbon Steel Substrate Using TIG Cladding Process. *Silicon*, *15*(18), 7733–7743. <https://doi.org/10.1007/s12633-023-02613-1>.

- Bansal, P., Singh, G., & Sidhu, H. S. (2020). Investigation of surface properties and corrosion behavior of plasma sprayed HA/ZnO coatings prepared on AZ31 Mg alloy. *Surface and Coatings Technology*, 401(August), 126241. <https://doi.org/10.1016/j.surfcoat.2020.126241>.
- Benea, L., Mardare-Danaila, E., Mardare, M., & Celis, J. P. (2014). Preparation of titanium oxide and hydroxyapatite on Ti-6Al-4V alloy surface and electrochemical behaviour in bio-simulated fluid solution. *Corrosion Science*, 80, 331–338. <https://doi.org/10.1016/j.corsci.2013.11.059>.
- Biswas, K., & Sahoo, C. K. (2023). A review on TIG cladding of engineering material for improving their surface property. *Surface Topography: Metrology and Properties*, 11(2). <https://doi.org/10.1088/2051-672X/acd6aa>.
- Breding, K., Jimbo, R., Hayashi, M., Xue, Y., Mustafa, K., & Andersson, M. (2014). The effect of hydroxyapatite nanocrystals on osseointegration of titanium implants: An in vivo rabbit study. *International Journal of Dentistry*, 2014. <https://doi.org/10.1155/2014/171305>.
- Buytoz, S., Ulutan, M., & Yildirim, M. M. (2005). Dry sliding wear behavior of TIG welding clad WC composite coatings. *Applied Surface Science*, 252(5), 1313–1323. <https://doi.org/10.1016/j.apsusc.2005.02.088>.
- Dikici, B., Ozdemir, I., & Topuz, M. (2016). Cold Spray Deposition of SS316L Powders on Al5052 Substrates: An Investigation on the Potential Using as Implant. *International Journal of Materials and Metallurgical Engineering*, 10(4), 483–487. <https://doi.org/doi.org/10.5281/zenodo.1124335>.
- Ebrahimi, N., Zadeh, A. S. A. H., Vaezi, M. R., & Mozafari, M. (2018). A new double-layer hydroxyapatite/alumina-silica coated titanium implants using plasma spray technique. *Surface and Coatings Technology*, 352(August), 474–482. <https://doi.org/10.1016/j.surfcoat.2018.08.022>.
- Eriksson, M., Andersson, M., Adolfsson, E., & Carlström, E. (2006). Titanium–hydroxyapatite composite biomaterial for dental implants. *Powder Metallurgy*, 49(1), 70–77. <https://doi.org/10.1179/174329006X94591>.
- Geetha, M., Singh, A. K., Asokamani, R., & Gogia, A. K. (2009). Ti based biomaterials, the ultimate choice for orthopaedic implants - A review. *Progress in Materials Science*, 54(3), 397–425. <https://doi.org/10.1016/j.pmatsci.2008.06.004>.
- Hodgson, A. W. E., Mueller, Y., Forster, D., & Virtanen, S. (2002). Electrochemical characterisation of passive films on Ti alloys under simulated biological conditions. *Electrochimica Acta*, 47(12), 1913–1923. [https://doi.org/10.1016/S0013-4686\(02\)00029-4](https://doi.org/10.1016/S0013-4686(02)00029-4).
- Hu, J., Ren, Y., Huang, Q., He, H., Liang, L., Liu, J., Li, R., & Wu, H. (2021). Microstructure and Corrosion Behavior of Ti-Nb Coatings on NiTi Substrate Fabricated by Laser Cladding. *Coatings*, 11(5), 597. <https://doi.org/10.3390/coatings11050597>.
- Ji, X., Zhao, M., Dong, L., Han, X., & Li, D. (2020). Influence of Ag/Ca ratio on the osteoblast growth and antibacterial activity of TiN coatings on Ti-6Al-4V by Ag and Ca ion implantation. *Surface and Coatings Technology*, 403(September), 126415. <https://doi.org/10.1016/j.surfcoat.2020.126415>.
- Kokubo, T., & Takadama, H. (2006). How useful is SBF in predicting in vivo bone bioactivity? *Biomaterials*, 27(15), 2907–2915. <https://doi.org/10.1016/j.biomaterials.2006.01.017>.
- Kumar, K., & Masanta, M. (2023). Effect of reducing heat input on autogenous TIG welding of Ti-6Al-4V alloy. *Transactions of Nonferrous Metals Society of China (English Edition)*, 33(12), 3712–3724. [https://doi.org/10.1016/S1003-6326\(23\)66365-4](https://doi.org/10.1016/S1003-6326(23)66365-4).
- Lucas, W. (1990). *TIG and Plasma welding*. *TIG and Plasma welding*. <https://doi.org/10.1533/9780857093264>.
- Mehl, C., Kern, M., Schütte, A. M., Kadem, L. F., & Selhuber-Unkel, C. (2016). Adhesion of living cells to abutment materials, dentin, and adhesive luting cement with different surface qualities. *Dental Materials*, 32(12), 1524–1535. <https://doi.org/10.1016/j.dental.2016.09.006>.
- Menzies, K. L., & Jones, L. (2010). The impact of contact angle on the biocompatibility of biomaterials. *Optometry and Vision Science*, 87(6), 387–399. <https://doi.org/10.1097/OPX.0b013e3181da863e>.
- Mohseni, E., Zalnezhad, E., Bushroa, A. R., Hamouda, A. M., Goh, B. T., & Yoon, G. H. (2015). Ti/TiN/HA coating on Ti-6Al-4V for biomedical applications. *Ceramics International*, 41(10), 14447–14457. <https://doi.org/10.1016/j.ceramint.2015.07.081>.

- Mohseni, E., Zalnezhad, E., & Bushroa, A. R. (2014). Comparative investigation on the adhesion of hydroxyapatite coating on Ti-6Al-4V implant: A review paper. *International Journal of Adhesion and Adhesives*, 48, 238–257. <https://doi.org/10.1016/j.ijadhadh.2013.09.030>.
- Nath, S., Tripathi, R., & Basu, B. (2009). Understanding phase stability, microstructure development and biocompatibility in calcium phosphate-titania composites, synthesized from hydroxyapatite and titanium powder mix. *Materials Science and Engineering C*, 29(1), 97–107. <https://doi.org/10.1016/j.msec.2008.05.019>.
- Niinomi, M., & Nakai, M. (2011). Titanium-Based Biomaterials for Preventing Stress Shielding between Implant Devices and Bone. *International Journal of Biomaterials*, 2011, 1–10. <https://doi.org/10.1155/2011/836587>.
- Niinomi, Mitsuo. (2002). Recent metallic materials for biomedical applications. *Metallurgical and Materials Transactions A*, 33(3), 477–486. <https://doi.org/10.1007/s11661-002-0109-2>.
- Padhee, C. K., Masanta, M., & Mondal, A. K. (2020). Feasibility of Al-TiC coating on AZ91 magnesium alloy by TIG alloying method for tribological application. *Transactions of Nonferrous Metals Society of China (English Edition)*, 30(6), 1550–1559. [https://doi.org/10.1016/S1003-6326\(20\)65318-3](https://doi.org/10.1016/S1003-6326(20)65318-3).
- Perl, D. P. (1985). Relationship of aluminum to Alzheimer's disease. *Environmental Health Perspectives*, VOL. 63(7), 149–153. <https://doi.org/10.1289/ehp.8563149>.
- Qiu, D., Yang, L., Yin, Y., & Wang, A. (2011). Preparation and characterization of hydroxyapatite/titania composite coating on NiTi alloy by electrochemical deposition. *Surface and Coatings Technology*, 205(10), 3280–3284. <https://doi.org/10.1016/j.surfcoat.2010.11.049>.
- Saroj, S., Sahoo, C. K., Tijo, D., Kumar, K., & Masanta, M. (2017). Sliding abrasive wear characteristic of TIG cladded TiC reinforced Inconel825 composite coating. *International Journal of Refractory Metals and Hard Materials*, 69(July), 119–130. <https://doi.org/10.1016/j.ijrmhm.2017.08.005>.
- Schultze, J. W., & Lohrengel, M. M. (2000). Stability, reactivity and breakdown of passive films. Problems of recent and future research. *Electrochimica Acta*, 45(15–16), 2499–2513. [https://doi.org/10.1016/S0013-4686\(00\)00347-9](https://doi.org/10.1016/S0013-4686(00)00347-9).
- Shbeh, M., Wally, Z. J., Elbadawi, M., Mosalagae, M., Al-Alak, H., Reilly, G. C., & Goodall, R. (2019). Incorporation of HA into porous titanium to form Ti-HA biocomposite foams. *Journal of the Mechanical Behavior of Biomedical Materials*, 96(April), 193–203. <https://doi.org/10.1016/j.jmbbm.2019.04.043>.
- Tijo, D., & Masanta, M. (2019). Effect of Ti/B4C ratio on the microstructure and mechanical characteristics of TIG cladded TiC-TiB2 coating on Ti-6Al-4V alloy. *Journal of Materials Processing Technology*, 266(October 2018), 184–197. <https://doi.org/10.1016/j.jmatprotec.2018.11.005>.
- Topuz, M., & Topuz, F. C. (2025). Nb₂CT_x MXene—Pistachio Shell-Filled Chitosan Coatings on Zn Biomaterial for In Vitro Corrosion and Bioactivity Improvement. *Coatings*, 15(10), 1210. <https://doi.org/10.3390/coatings15101210>.
- Topuz, M., & Teter, N. (2025). The Effect of Hydroxyapatite Fraction in Titanium—Hydroxyapatite Composite Coatings on Ti-6Al-4V Alloy With TIG Cladding. *Materials and Corrosion, Early View*, 1–13. <https://doi.org/10.1002/maco.70045>.
- Topuz, M., Topuz, F. C., Dikici, B., & Seifzadeh, D. (2025). Sustainable Walnut Shell-Filled Polylactic Acid–Hydroxyapatite Hybrid Coatings for Enhanced Corrosion Resistance and Bioactivity of Magnesium Biomaterials. *Journal of Applied Polymer Science*, 142(33), e57321. <https://doi.org/10.1002/app.57321>.
- Topuz, M., Akinay, Y., Karatas, E., & Cetin, T. (2024a). Ti₃C₂T_x MXene-functionalized Hydroxyapatite/Halloysite nanotube filled poly– (lactic acid) coatings on magnesium: In vitro and antibacterial applications. *Journal of Magnesium and Alloys*, 12(9), 3758–3771. <https://doi.org/10.1016/j.jma.2024.09.017>.
- Topuz, M., Dikici, B., Kasapoglu, A. E., Zhao, X., & Niinomi, M. (2024b). Systematic characterization and enhanced corrosion resistance of novel β-type Ti-30Zr-5Mo biomedical alloys with halloysite nanotubes (HNTs) and zirconia (ZrO₂)-reinforced polylactic acid (PLA) matrix coatings. *Materials Today Communications*, 40(July), 110110. <https://doi.org/10.1016/j.mtcomm.2024.110110>.
- Topuz, M. (2023a). Hydroxyapatite – Al₂O₃ reinforced poly– (lactic acid) hybrid coatings on magnesium: Characterization, mechanical and in-vitro bioactivity properties. *Surfaces and Interfaces*, 37(January), 102724. <https://doi.org/10.1016/j.surf.2023.102724>.
- Topuz, M. (2023b). Investigation of Halloysite Nanotube Effect in Poly– (Lactic acid)/Hydroxyapatite Coatings on

Ti-6Al-4V Biomedical Alloy. *Journal of Polymers and the Environment*, 31(9), 4112–4126. <https://doi.org/10.1007/s10924-023-02926-7>.

Topuz, M., Yigit, O., Kaseem, M., & Dikici, B. (2023). Synthesis of implantable ceramic coatings and their properties. In A. Gupta, Ram K. Motallebzadeh, Amir Kakooei, Saeid Nguyen, Tua Anh Behera (Ed.), *Advanced Ceramic Coatings for Biomedical Applications* (Vol. 13, pp. 53–86). Elsevier. <https://doi.org/10.1016/B978-0-323-99626-6.00008-1>.

Topuz, M., Dikici, B., & Gavgali, M. (2021a). Titanium-based composite scaffolds reinforced with hydroxyapatite-zirconia: Production, mechanical and in-vitro characterization. *Journal of the Mechanical Behavior of Biomedical Materials*, 118(January), 104480. <https://doi.org/10.1016/j.jmbbm.2021.104480>.

Topuz, M., Dikici, B., Gavgali, M., & Kaseem, M. (2021b). Processing of Ti/(HA+ZrO₂) biocomposite and 50% porous hybrid scaffolds with low Young's modulus by powder metallurgy: Comparing of structural, mechanical, and corrosion properties. *Materials Today Communications*, 29(August), 102813. <https://doi.org/10.1016/j.mtcomm.2021.102813>.

Tozkoparan, B., Dikici, B., Topuz, M., Bedir, F., & Gavgali, M. (2020). Al-5Cu/B4Cp composites: The combined effect of artificially aging (T6) and particle volume fractions on the corrosion behaviour. *Advanced Powder Technology*, 31(7), 2833–2842. <https://doi.org/10.1016/j.apt.2020.05.006>.

Waghmare, D. T., Kumar Padhee, C., Prasad, R., & Masanta, M. (2018). NiTi coating on Ti-6Al-4V alloy by TIG cladding process for improvement of wear resistance: Microstructure evolution and mechanical performances. *Journal of Materials Processing Technology*, 262(January), 551–561. <https://doi.org/10.1016/j.jmatprotec.2018.07.033>.

Weng, F., Chen, C., & Yu, H. (2014). Research status of laser cladding on titanium and its alloys: A review. *Materials and Design*, 58, 412–425. <https://doi.org/10.1016/j.matdes.2014.01.077>.